ARTICLES
PUBLISHED ONLINE: 14 DECEMBER 2015 | DOI: 10.1038/NPHYS3584
nature physics

A Thouless quantum pump with ultracold bosonic atoms in an optical superlattice

M. Lohse[1,2]*, C. Schweizer[1,2], O. Zilberberg[3], M. Aidelsburger[1,2] and I. Bloch[1,2]

Topological charge pumping enables the transport of charge through an adiabatic cyclic evolution of the underlying Hamiltonian. In contrast to classical transport, the transported charge is quantized and purely determined by the topology of the pump cycle, making it robust to perturbations. Here, we report on the realization of such a pump with ultracold bosonic atoms forming a Mott insulator in a dynamically controlled optical superlattice. By taking *in situ* images of the cloud, we observe a quantized deflection per pump cycle. We reveal the pump's genuine quantum nature by showing that, in contrast to ground-state particles, a counterintuitive reversed deflection occurs for particles in the first excited band. Furthermore, we directly demonstrate that the system undergoes a controlled topological transition in higher bands when tuning the superlattice parameters. These results open a route to the implementation of more complex pumping schemes, including spin degrees of freedom and higher dimensions.

The concept of a topological charge pump was introduced by Thouless[1] who showed that a slow cyclic variation of a periodic potential can give rise to a quantized motion of particles that is topologically protected against perturbations[2]. On a fundamental level, the charge that is transported per pump cycle can be connected to a topological invariant, the Chern number, first introduced in the context of the integer quantum Hall effect[3,4]. A Thouless quantum pump may therefore be regarded as a 'dynamical' version of the integer quantum Hall effect. In solid-state systems, charge pumping has received much attention, mainly due to its potential for realizing novel current standards[5,6], but also for characterizing many-body systems[7,8]. Quantized transport of electrons without an external bias was observed in tunnel junctions with modulated gate voltages[9], in 1D channels using surface acoustic waves[10] and in quantum dots[11]. Whereas the latter was used to realize an adiabatic quantum pump[12,13], topological charge pumping has so far remained out of reach in condensed matter experiments. In engineered bosonic systems, non-quantized topological pumping of edge states was observed in 1D quasicrystalline photonic waveguide arrays[14,15]. In cold atomic systems, topological Bloch bands have been realized, ranging from the Su–Schrieffer–Heeger (SSH) model[16], the Hofstadter model in real space[17,18] and synthetic dimensions[19,20], to the Haldane model[21]. Their geometric features have been probed using novel interferometric[16,22] and transport probes[21,23] that have, for example, enabled the direct measurement of the Chern number through bulk topological currents[23].

Due to their versatility, ultracold atoms in optical superlattices constitute an ideal system for the implementation of quantized topological charge pumps[24–26]. A superlattice is formed by superimposing two lattices with periodicities d_l and $d_s = \alpha d_l$, $\alpha < 1$. This creates a potential $V_s \sin^2(\pi x/d_s + \pi/2) + V_l \sin^2(\pi x/d_l - \varphi/2)$, where V_s (V_l) denotes the depth of the short (long) lattice, respectively. The relative position of the lattices is determined by the variable phase φ. When applying Bloch's theorem, the resulting single-particle Hamiltonian $\hat{\mathcal{H}}(k_x, \varphi)$ is periodic in both the quasi-momentum $k_x \in]-\pi/d_l, \pi/d_l]$ and the superlattice phase φ.

A cyclic pumping scheme can be realized by adiabatically varying φ where one cycle corresponds to a change of 2π, that is, moving the long lattice by d_l. A particle which is initially in an eigenstate $|u_n(k_x, \varphi_0)\rangle$ of $\hat{\mathcal{H}}(k_x, \varphi_0)$ in the nth band follows the corresponding instantaneous eigenstate $|u_n(k_x, \varphi)\rangle$. Even with perfect adiabaticity, however, the particle acquires a small admixture of states from other bands, proportional to $\partial_t \varphi$. This gives rise to an anomalous velocity $\dot{x}_n = \Omega_n \partial_t \varphi$, determined by the Berry curvature $\Omega_n(k_x, \varphi) = i\big(\langle \partial_\varphi u_n | \partial_{k_x} u_n \rangle - \langle \partial_{k_x} u_n | \partial_\varphi u_n \rangle\big)$ (refs 27,28). Hence, changing φ induces a motion of the particle which, depending on the sign of Ω_n, is either in the same or opposite direction as the moving lattice. The displacement after one cycle is obtained by integrating $\dot{x}_n$ and can in principle take any arbitrary value.

For a filled or homogeneously populated band, however, the average displacement of the entire cloud per cycle can be related to a 2D topological invariant, the Chern number ν_n of the pumping process:

$$\nu_n = \frac{1}{2\pi} \int_{\mathrm{FBZ}} \int_0^{2\pi} \Omega_n(k_x, \varphi) \mathrm{d}\varphi \mathrm{d}k_x \qquad (1)$$

Here, FBZ denotes the first Brillouin zone of the superlattice. Such a case can be realized with both fermions, by placing the Fermi energy in a band gap, and bosons, by preparing a Mott insulator in the nth band as in our experiment. During one cycle, the cloud's centre-of-mass (COM) position changes by $\nu_n d_l$ and is quantized in units of d_l because ν_n can only take integer values. Unlike in classical systems, this motion can be faster ($\nu_n > 1$) or even opposite ($\nu_n < 0$) compared to the one of the underlying lattice[29]. As the displacement is proportional to a topological invariant, it neither depends on the pumping speed, provided adiabaticity still holds, nor on the specific lattice parameters as long as band crossings do not occur. Hence, the transport is highly robust against perturbations such as

[1]Fakultät für Physik, Ludwig-Maximilians-Universität, Schellingstrasse 4, 80799 München, Germany. [2]Max-Planck-Institut für Quantenoptik, Hans-Kopfermann-Strasse 1, 85748 Garching, Germany. [3]Institut für Theoretische Physik, ETH Zürich, 8093 Zürich, Switzerland.
*e-mail: michael.lohse@physik.uni-muenchen.de

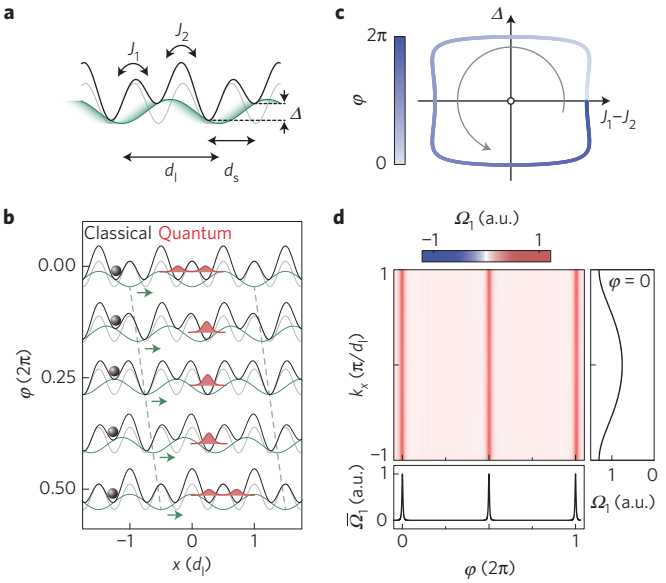

Figure 1 | Topological charge pumping in an optical superlattice. **a**, Superlattice potential created by superimposing two lattices with periodicities d_l and $d_s = d_l/2$. Here, J_1 and J_2 denote the tunnel couplings and Δ the energy offset between neighbouring sites. **b**, Evolution of the ground-state Wannier function (red) during the first half of a pump cycle. The long lattice is shifted to the right when increasing the superlattice phase φ. An atom initially localized in a symmetric superposition on a double well tunnels to the lower-lying site and thereby follows the motion of the long lattice in a quantized fashion. A classical particle, on the other hand, stays at a fixed position as the individual sites do not move. **c**, Pump cycle in the $(J_1\text{–}J_2)-\Delta$ parameter space. Varying φ from 0 to 2π corresponds to a closed path around the degeneracy point at the origin where $\Delta = 0$ and $J_1 = J_2$. **d**, Berry curvature Ω_1 of the lowest band as a function of φ and the quasi-momentum k_x for a lattice with $V_s = 10E_{r,s}$ and $V_l = 20E_{r,l}$, where $E_{r,i}, i \in \{s, l\}$ denotes the corresponding recoil energy. The panel below shows the Berry curvature averaged along k_x, as seen by a particle localized in a single double well, which is peaked at the symmetric double well configurations $\varphi = l\pi, l \in \mathbb{Z}$. The graph on the right shows $\Omega_1(k_x)$ for $\varphi = 0$.

interaction effects in fermionic systems or disorder[2]. In particular, a weak harmonic confinement only leads to exponentially small corrections[30] and does not affect the relation between the COM shift and the Chern number[31].

The connection to a Chern topological invariant shows that charge pumping in a 1D superlattice is closely related to the integer quantum Hall effect, where charged particles move in 2D in the presence of a perpendicular magnetic field. Indeed, the adiabatic variation of φ is equivalent to the threading of magnetic flux through a cylinder[1] that generates an electric field in the orthogonal direction and leads to the quantized Hall conductance[4]. A direct analogy between these systems can be made in two limiting cases: the quantum sliding lattice with $V_s \to 0$ and the deep tight-binding limit with $V_s \gg V_l^2/(4E_{r,s})$, where $E_{r,s} = h^2/(2m_a\lambda_s^2)$ denotes the recoil energy of the short lattice, m_a the mass of an atom and λ_s the respective wavelength. The former case matches with the free particle limit of Landau levels that are associated with Chern numbers $\nu_n = +1$. In this limit, one can understand the pumping by following Laughlin's argument[32], where the threading of the magnetic flux leads to a sliding of the localized oscillator centres. In the latter, one obtains the generalized 1D Harper model[33,34] which, using dimensional extension[35,36], can be mapped onto the 2D Harper–Hofstadter–Hatsugai (HHH) model describing non-interacting particles on a 2D square lattice with a uniform magnetic flux $2\pi\alpha$ and nearest- as well as next-nearest-neighbour hopping[33,37–39] (see Supplementary Information). In this mapping, φ corresponds to the transverse quasimomentum k_y. In the following, unless mentioned otherwise, we will focus on the Wannier tunnelling regime $V_s \gtrsim V_l^2/(4E_{r,s})$ where—even though the direct mapping to the 1D Harper model breaks down—the pump is characterized by the same Chern number distribution.

In the experiment, we use a superlattice with $d_l = 2d_s$ and two sites per unit cell (Fig. 1a). In the tight-binding limit, it is described by the Rice–Mele Hamiltonian[40]

$$\hat{H}(\varphi) = -\sum_m \left(J_1(\varphi)\hat{b}_m^\dagger \hat{a}_m + J_2(\varphi)\hat{a}_{m+1}^\dagger \hat{b}_m + \text{h.c.}\right) + \frac{\Delta(\varphi)}{2}\sum_m \left(\hat{a}_m^\dagger \hat{a}_m - \hat{b}_m^\dagger \hat{b}_m\right) \quad (2)$$

where $\hat{a}_m^\dagger$ ($\hat{a}_m$) and $\hat{b}_m^\dagger$ ($\hat{b}_m$) are the creation (annihilation) operators acting on the even (left) and odd (right) site of the mth unit cell, respectively. J_1, J_2 denote the tunnel couplings and Δ the energy offset between neighbouring sites. For $\Delta = 0$, this Hamiltonian reduces to the SSH model[41].

The mechanism underlying the pumping can also be understood on a microscopic level. Shifting the phase φ changes the shape of the potential (Fig. 1b) and modifies J_1, J_2 and Δ periodically (Fig. 1c). At $\varphi = 0$ ($\Delta = 0$, $J_1 > J_2$), a ground-state particle localized in a single double well is initially in a symmetric superposition of residing on both the left and right sites. With increasing φ, that is, shifting the long lattice to the right, the double wells are tilted ($\Delta > 0$) and the atom tunnels to the lower-lying site on the right. The sign of $J_1\text{–}J_2$ is reversed at $\varphi = \pi/2$, where the tilt is largest, and at $\varphi = \pi$ the lattice forms symmetric double wells again, but shifted by one short lattice constant to the right. The atom, which remained on the lower site for large Δ, delocalizes over the shifted double well as Δ becomes comparable to J_2 and therefore has moved by $d_l/2$ during the first half of the pump cycle. In the second half, the same procedure is repeated, but shifted by one site. After one cycle, the lattice configuration is identical to the starting point, but the atom ends up in the double well next to the initial one. In contrast to this, a classical particle would not move because the positions of the individual sites do not change. This illustrates the importance of quantum tunnelling for the pumping.

During the pump cycle, the system moves along a closed trajectory in the $(J_1\text{–}J_2)-\Delta$ parameter space. It encircles the degeneracy point at $\Delta = 0$ and $J_1 = J_2$, where the two bands of the Rice–Mele model touch, and smoothly connects the topologically distinct phases $J_1 < J_2$ and $J_1 > J_2$ of the SSH model (Fig. 1c). The Berry curvature and thus the motion of the atoms peak around $\varphi = l\pi, l \in \mathbb{Z}$ where the tilt changes sign and the atoms tunnel to the neighbouring sites (Fig. 1d). The Chern numbers of the pump cycles in the two bands of this model are $\nu_1 = +1$ and $\nu_2 = -1$, giving the same Chern number distribution as the HHH model with $\alpha = 1/2$ (ref. 39). Their sum vanishes because these bands emerge from the topologically trivial lowest Bloch band of the short lattice.

The experimental sequence starts by preparing an $n = 1/2$ Mott insulator of ^{87}Rb atoms in a 3D optical lattice with at most one atom per unit cell in the ground state of symmetric double wells with $\varphi = 0$ and $J_1 \gg J_2$ (see Methods). Due to the large on-site interaction, each atom is localized on an individual double well, resulting in a homogeneous delocalization over the entire first Brillouin zone. The pumping is performed by adiabatically shifting the phase φ of the long lattice (see Methods) and the resulting motion of the atoms is tracked by measuring the COM position of the cloud *in situ*. The displacement during one cycle is indeed quantized and occurs in steps (Fig. 2a)—unlike the underlying linear motion of the long lattice. The cloud moves by one lattice constant d_l

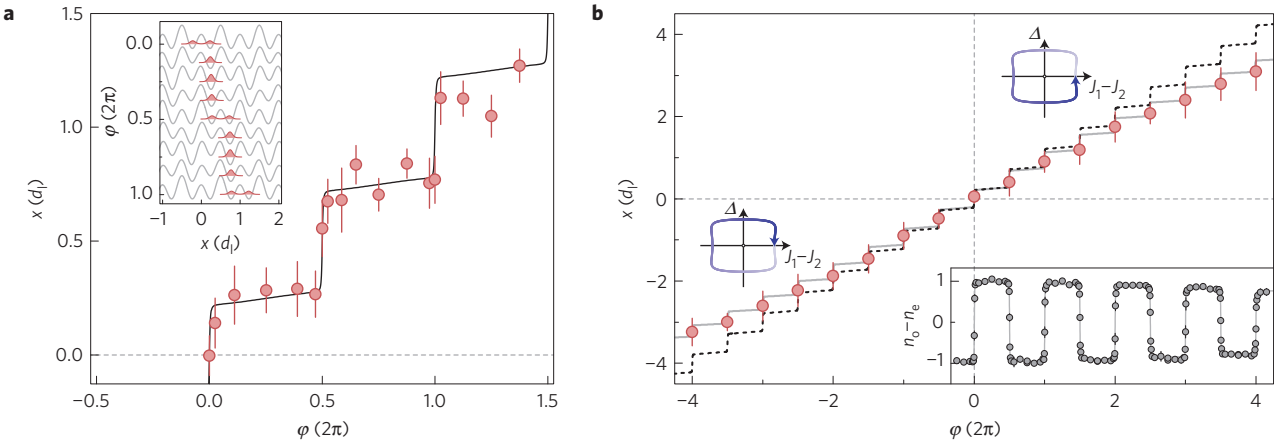

Figure 2 | Centre-of-mass (COM) position of the atom cloud as a function of the pumping parameter φ for the lowest band with $V_s = 10.0(3)E_{r,s}$ and $V_l = 20(1)E_{r,l}$. a, Detailed evolution of the measured COM position during a pump cycle. The step-like motion is caused by tunnelling of the atoms to the lower-lying sites. The solid black line depicts the calculated COM motion of a localized Wannier function. Each point is the average of ten data sets and the error bar shows the error of the mean. COM positions are determined differentially comparing a sequence with pumping to a reference sequence of the same length, but with constant phase $\varphi = 0$. One data set is obtained by averaging ten images, taken in alternating order, and subtracting the resulting COM positions. Inset, The motion of a localized Wannier function in the first band during a full pump cycle. **b**, COM displacement and site populations for multiple pump cycles in the positive and negative pumping direction. The COM positions are averaged over ten data sets and the error bars depict the standard deviation. The dashed black line shows the ideal motion of a localized Wannier function and the grey line is a fit of the Wannier COM to the data assuming a finite pumping efficiency of 97.9(2)% per each half of a pump cycle (see Supplementary Information). Inset, The population imbalance between even and odd sites as a function of φ with n_e (n_o) the fraction of atoms on even (odd) sites. Each data point is the average of five measurements and the error bars indicate the corresponding standard deviation. The grey line is obtained by fitting the calculated even–odd distribution of the Wannier function using the same model as for the COM displacement which yields an efficiency of 98.7(1)% leading to a slight decrease of the imbalance over time.

per cycle as expected for $\nu_1 = +1$ and the steps appear around $\varphi = l\pi, l \in \mathbb{Z}$, where the atoms tunnel from one side of the double wells to the other. When performing multiple cycles the cloud keeps moving to the right, whereas it propagates in the opposite direction for the reversed pumping direction $\varphi < 0$ (Fig. 2b). The small deviation from the expected displacement for the motion of ideal Wannier functions can be attributed to a finite pumping efficiency due to non-adiabatic band transitions and the additional trapping potential, whereas thermal effects caused by the finite temperature of the atoms are negligible (see Supplementary Information).

The step-like transport behaviour can also be observed in site-resolved band mapping measurements (inset of Fig. 2b), which determine the number of atoms on even and odd sites. As for the COM position, a step occurs in the even–odd distribution whenever a symmetric double-well configuration is crossed at $\varphi = l\pi, l \in \mathbb{Z}$. Using the measured even–odd fractions, one can estimate the transfer efficiency, that is, the fraction of atoms transferred from site i to $i+1$ at each step. This is equivalent to the fraction staying in the lowest band during one half of the pump cycle and allows to quantify the adiabaticity of the pumping protocol. From our data we obtain an efficiency of 98.7(1)% (see Supplementary Information). With the same model, the ideal COM displacement can be fitted to the measured positions which yields an efficiency of 97.9(2)%. The small additional reduction is probably caused by the trap which can induce non-adiabatic transitions between neighbouring double wells at the edges of the cloud (see Supplementary Information).

Due to the topological nature of the pumping, the displacement per cycle for the lowest band does not depend on the path in the $(J_1-J_2)-\Delta$ plane as long as it encompasses the degeneracy point. Moreover, it is independent of V_s as the sliding lattice and the tight-binding Thouless pump are topologically equivalent for the first band and connected by a smooth crossover without closing the gap to the second band. To verify this, we measured the deflection of the cloud with $V_l = 25(1)E_{r,l}$ for various values of V_s. For all parameters, the resulting displacements are consistent within the error bars (Fig. 3).

The excited band in the Rice–Mele model exhibits counter-propagating charge pumping with $\nu_2 = -1$, that is, the atoms are expected to move in the opposite direction to the long lattice. This

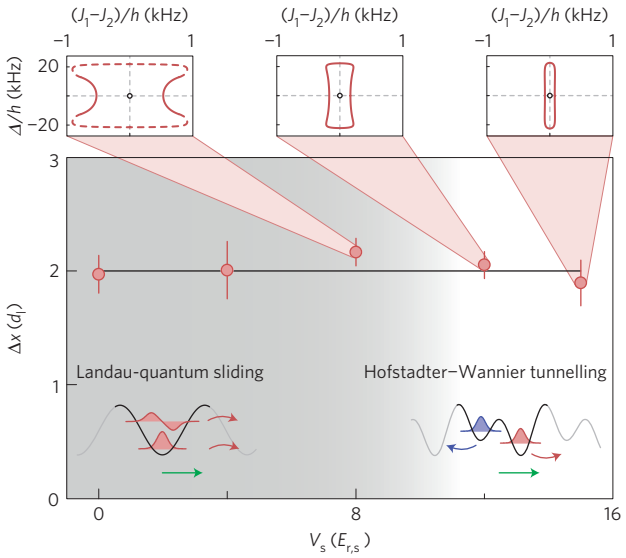

Figure 3 | Transition from a quantum sliding lattice to the Wannier tunnelling limit for the lowest band. Differential deflection $\Delta x = x_+ - x_-$ between positive (x_+) and negative pumping direction (x_-) after one pump cycle for various lattice depths V_s at $V_l = 25(1)\,E_{r,l}$. Each point consists of ten data sets comparing the COM position of ten averaged images for both directions. The error bars depict the error of the mean. For the data points in the tight-binding regime, the insets show the corresponding pump cycles in the $(J_1-J_2)-\Delta$ parameter space. For $V_s = 8E_{r,s}$, the two-band model breaks down for large tilts such that J_1, J_2 and Δ are not well-defined. The dashed line therefore connects the points where the gap between the second and third band becomes smaller than $10J_1$ for $\varphi = 0$.

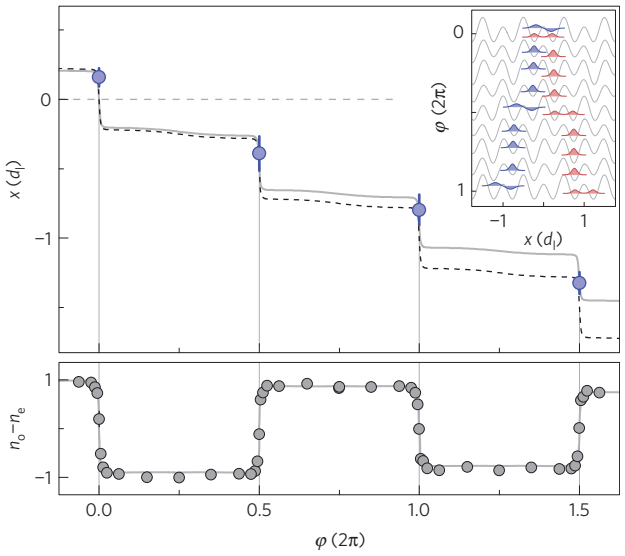

Figure 4 | Cloud displacement and site occupations for the first excited band with $V_s = 10.0(3)E_{r,s}$ and $V_l = 20(1)E_{r,l}$. The main plot shows the evolution of the COM position for up to 1.5 pump cycles. The data points are averaged over ten data sets with the errors being the error of the mean. The dashed black line indicates the motion of a localized Wannier function of the second band and the grey line is a fit to the data using the same model as in Fig. 2b, giving a transfer efficiency of 97(2)%. The inset illustrates the evolution of the Wannier functions of the first and second band during a pump cycle, showing a deflection in opposite directions. The lower plot shows the imbalance of the fraction of atoms on even (n_e) and odd sites (n_o) averaged over 3–6 measurements each with the error bars depicting the standard deviation. The grey line is a fit of the even–odd distribution of the corresponding Wannier functions with a pumping efficiency of 96.7(3)% (see Supplementary Information).

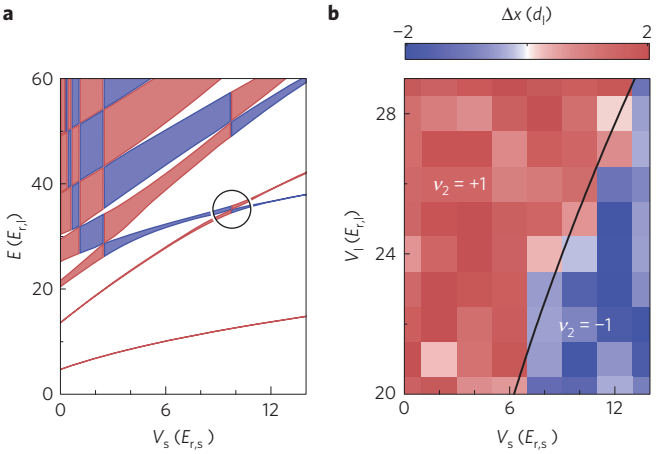

Figure 5 | Topological transition in the first excited band. a, Band structure at $\varphi = 0.5\pi$, where the band crossings occur, and Chern number distribution versus V_s with $V_l = 25E_{r,l}$. The shaded areas illustrate the width of the Bloch bands, which were calculated by numerical diagonalization of $\hat{\mathcal{H}}(k_x, \varphi)$. The colour indicates the Chern number of the corresponding pump cycle with red being +1 and blue −1. Starting from alternating Chern numbers in the Wannier tunnelling limit for large V_s, the negative Chern numbers successively propagate towards higher bands in a series of topological transitions when lowering V_s, giving rise to a uniform distribution with $\nu_n = +1$ in the Landau limit of a sliding long lattice. The circle highlights the crossing of the 2nd and 3rd band leading to the topological transition studied in **b**. **b**, Differential deflection $\Delta x = x_+ - x_-$ between single pump cycles in opposite directions (x_+, x_-) for the second band as a function of the lattice depths V_s and V_l. At small V_s, $\nu_2 = +1$ and atoms move in the same direction as the lattice, but as V_s increases a topological transition occurs at $V_s = V_l^2/(4E_{r,s})$, indicated by the black line, where ν_2 suddenly changes to −1 and the direction of motion is reversed. Each square corresponds to one data set averaged over 10–12 pairs of images.

underlines the pump's intrinsic quantum mechanical character as such a motion could not occur for classical particles. To study this, the atoms were prepared in the second band at $\varphi = 0$ (see Methods) and pumping was performed with identical parameters as for the first band in Fig. 2. When moving the lattice to the right ($\varphi > 0$), the cloud indeed shifts to the left with $x < 0$ (Fig. 4). This is further confirmed by the measured site occupations, showing that the behaviour is exactly reversed compared with the lowest band. Whereas the first band is localized on the lower site for large Δ, atoms in the second band are found on the upper site and are therefore transported in the opposite direction. The slightly larger deviation from theory is mostly due to the finite lifetime of atoms in the higher band. This leads to a lower transfer efficiency of 96.7(3)% obtained from the site populations, in agreement with the value from the fit to the COM positions of 97(2)% (see Supplementary Methods).

By varying V_s/V_l^2, one can study the transition between the topologically very different regimes of the sliding long lattice with $V_s = 0E_{r,s}$ and the Wannier tunnelling limit for $V_s > V_l^2/(4E_{r,s})$. For the latter, the Chern numbers of the bands alternate between $\nu_{2n+1} = +1$ and $\nu_{2n} = -1$ for $d_l = 2d_s$, like in the HHH model with a flux of π. This causes the opposite deflections for the first and second band observed in Figs 2 and 4. In the other limit $V_s \to 0E_{r,s}$, however, each band corresponds to a single Landau level with $\nu_n = +1$. Between these two limiting cases, as V_s is decreased, an infinite series of topological transitions occurs where two bands touch and exchange their Chern numbers (Fig. 5a). Thereby the negative ν_n are successively transferred to higher bands and they become positive for the lower bands.

Although the deflection in the first band is independent of V_s, there is a transition for the second band where the gap to the third band closes and ν_2 changes from −1 to +1. This transition can be mapped out by measuring the displacement of the cloud as a function of the lattice depths V_s and V_l (Fig. 5b). The direction of the motion reverses when crossing the transition, which occurs at $V_s = V_l^2/(4E_{r,s})$ in the tight-binding limit. For small V_s, atoms in the second band move in the same direction as the lattice, whereas they move in the opposite direction in the Wannier tunnelling regime.

In conclusion, we have demonstrated the implementation of a topological charge pump using ultracold atoms. Unlike previous experiments studying non-quantized pumping of edge states, we observe a quantized response in the bulk. Combining such a pump with novel techniques for engineering optical potentials at the single-site level[42,43] would allow for a direct observation of edge states in finite systems[44] and the study of their transport properties[14]. Furthermore, by adjusting the ratio of the lattice constants $\alpha = d_s/d_l$, one can realize a wide variety of commensurate and incommensurate superlattices where the Chern number of the lowest band can in principle take arbitrary integer values. In addition to the negative deflection for $\nu_n < 0$ shown here, another counterintuitive case of charge pumping can occur in these systems where the atoms move faster than the long lattice for $\nu_n > 1$ (ref. 29). By adding a spin degree of freedom, the pumping scheme can be used to implement the Z_2 spin pump[45,46] in a spin-dependent superlattice[47]. Moreover, extending the Thouless pump to 2D systems would enable the realization of an analogon of the 4D integer quantum Hall effect[36,48].

Note added in proof: Recently, we became aware of similar work by S. Nakajima *et al.*[49] implementing the Thouless pump with fermionic atoms.

Methods

Methods and any associated references are available in the online version of the paper.

Received 8 July 2015; accepted 5 November 2015; published online 14 December 2015

References

1. Thouless, D. J. Quantization of particle transport. *Phys. Rev. B* **27,** 6083–6087 (1983).
2. Niu, Q. & Thouless, D. J. Quantised adiabatic charge transport in the presence of substrate disorder and many-body interaction. *J. Phys. A* **17,** 2453 (1984).
3. Klitzing, K. V., Dorda, G. & Pepper, M. New method for high-accuracy determination of the fine-structure constant based on quantized Hall resistance. *Phys. Rev. Lett.* **45,** 494–497 (1980).
4. Thouless, D., Kohmoto, M., Nightingale, M. & den Nijs, M. Quantized Hall conductance in a two-dimensional periodic potential. *Phys. Rev. Lett.* **49,** 405–408 (1982).
5. Niu, Q. Towards a quantum pump of electric charges. *Phys. Rev. Lett.* **64,** 1812–1815 (1990).
6. Pekola, J. P. *et al.* Single-electron current sources: Toward a refined definition of the ampere. *Rev. Mod. Phys.* **85,** 1421–1472 (2013).
7. Splettstoesser, J., Governale, M., König, J. & Fazio, R. Adiabatic pumping through interacting quantum dots. *Phys. Rev. Lett.* **95,** 246803 (2005).
8. Marra, P., Citro, R. & Ortix, C. Fractional quantization of the topological charge pumping in a one-dimensional superlattice. *Phys. Rev. B* **91,** 125411 (2015).
9. Pothier, H., Lafarge, P., Urbina, C., Esteve, D. & Devoret, M. H. Single-electron pump based on charging effects. *Europhys. Lett.* **17,** 249 (1992).
10. Talyanskii, V. I. *et al.* Single-electron transport in a one-dimensional channel by high-frequency surface acoustic waves. *Phys. Rev. B* **56,** 15180–15184 (1997).
11. Blumenthal, M. D. *et al.* Gigahertz quantized charge pumping. *Nature Phys.* **3,** 343–347 (2007).
12. Switkes, M., Marcus, C. M., Campman, K. & Gossard, A. C. An adiabatic quantum electron pump. *Science* **283,** 1905–1908 (1999).
13. Brouwer, P. W. Scattering approach to parametric pumping. *Phys. Rev. B* **58,** R10135 (1998).
14. Kraus, Y. E., Lahini, Y., Ringel, Z., Verbin, M. & Zilberberg, O. Topological states and adiabatic pumping in quasicrystals. *Phys. Rev. Lett.* **109,** 106402 (2012).
15. Verbin, M., Zilberberg, O., Lahini, Y., Kraus, Y. E. & Silberberg, Y. Topological pumping over a photonic Fibonacci quasicrystal. *Phys. Rev. B* **91,** 064201 (2015).
16. Atala, M. *et al.* Direct measurement of the Zak phase in topological Bloch bands. *Nature Phys.* **9,** 795–800 (2013).
17. Aidelsburger, M. *et al.* Realization of the Hofstadter Hamiltonian with ultracold atoms in optical lattices. *Phys. Rev. Lett.* **111,** 185301 (2013).
18. Miyake, H., Siviloglou, G. A., Kennedy, C. J., Burton, W. C. & Ketterle, W. Realizing the Harper Hamiltonian with laser-assisted tunneling in optical lattices. *Phys. Rev. Lett.* **111,** 185302 (2013).
19. Mancini, M. *et al.* Observation of chiral edge states with neutral fermions in synthetic Hall ribbons. *Science* **349,** 1510–1513 (2015).
20. Stuhl, B. K., Lu, H.-I., Aycock, L. M., Genkina, D. & Spielman, I. B. Visualizing edge states with an atomic Bose gas in the quantum Hall regime. *Science* **349,** 1514–1518 (2015).
21. Jotzu, G. *et al.* Experimental realization of the topological Haldane model with ultracold fermions. *Nature* **515,** 237–240 (2014).
22. Duca, L. *et al.* An Aharonov–Bohm interferometer for determining Bloch band topology. *Science* **347,** 288–292 (2015).
23. Aidelsburger, M. *et al.* Measuring the Chern number of Hofstadter bands with ultracold bosonic atoms. *Nature Phys.* **11,** 162–166 (2015).
24. Romero-Isart, O. & García-Ripoll, J. J. Quantum ratchets for quantum communication with optical superlattices. *Phys. Rev. A* **76,** 052304 (2007).
25. Qian, Y., Gong, M. & Zhang, C. Quantum transport of bosonic cold atoms in double-well optical lattices. *Phys. Rev. A* **84,** 013608 (2011).
26. Wang, L., Troyer, M. & Dai, X. Topological charge pumping in a one-dimensional optical lattice. *Phys. Rev. Lett.* **111,** 026802 (2013).
27. Karplus, R. & Luttinger, J. M. Hall effect in ferromagnetics. *Phys. Rev.* **95,** 1154–1160 (1954).
28. Xiao, D., Chang, M.-C. & Niu, Q. Berry phase effects on electronic properties. *Rev. Mod. Phys.* **82,** 1959–2007 (2010).
29. Wei, R. & Mueller, E. J. Anomalous charge pumping in a one-dimensional optical superlattice. *Phys. Rev. A* **92,** 013609 (2015).
30. Ringel, Z. & Kraus, Y. E. Determining topological order from a local ground-state correlation function. *Phys. Rev. B* **83,** 245115 (2011).
31. Wang, L., Soluyanov, A. A. & Troyer, M. Proposal for direct measurement of topological invariants in optical lattices. *Phys. Rev. Lett.* **110,** 166802 (2013).
32. Laughlin, R. B. Quantized Hall conductivity in two dimensions. *Phys. Rev. B* **23,** 5632–5633 (1981).
33. Harper, P. G. The general motion of conduction electrons in a uniform magnetic field, with application to the diamagnetism of metals. *Proc. Phys. Soc. A* **68,** 879 (1955).
34. Roux, G. *et al.* Quasiperiodic Bose–Hubbard model and localization in one-dimensional cold atomic gases. *Phys. Rev. A* **78,** 023628 (2008).
35. Kraus, Y. E. & Zilberberg, O. Topological equivalence between the Fibonacci quasicrystal and the Harper model. *Phys. Rev. Lett.* **109,** 116404 (2012).
36. Kraus, Y. E., Ringel, Z. & Zilberberg, O. Four-dimensional quantum Hall effect in a two-dimensional quasicrystal. *Phys. Rev. Lett.* **111,** 226401 (2013).
37. Azbel, M. Y. Energy spectrum of a conduction electron in a magnetic field. *Zh. Eksp. Teor. Fiz.* **46,** 929–946 (1964) [*Sov. Phys. JETP* **19**, 634–645 (1964)].
38. Hofstadter, D. R. Energy levels and wave functions of Bloch electrons in rational and irrational magnetic fields. *Phys. Rev. B* **14,** 2239–2249 (1976).
39. Hatsugai, Y. & Kohmoto, M. Energy spectrum and the quantum Hall effect on the square lattice with next-nearest-neighbor hopping. *Phys. Rev. B* **42,** 8282–8294 (1990).
40. Rice, M. J. & Mele, E. J. Elementary excitations of a linearly conjugated diatomic polymer. *Phys. Rev. Lett.* **49,** 1455–1459 (1982).
41. Su, W. P., Schrieffer, J. R. & Heeger, A. J. Solitons in polyacetylene. *Phys. Rev. Lett.* **42,** 1698–1701 (1979).
42. Weitenberg, C. *et al.* Single-spin addressing in an atomic Mott insulator. *Nature* **471,** 319–324 (2011).
43. Preiss, P. M. *et al.* Strongly correlated quantum walks in optical lattices. *Science* **347,** 1229–1233 (2015).
44. Kitagawa, T. *et al.* Observation of topologically protected bound states in photonic quantum walks. *Nature Commun.* **3,** 882 (2012).
45. Shindou, R. Quantum spin pump in $s=1/2$ antiferromagnetic chains-holonomy of phase operators in sine-Gordon theory. *J. Phys. Soc. Jpn* **74,** 1214–1223 (2005).
46. Fu, L. & Kane, C. L. Time reversal polarization and a Z_2 adiabatic spin pump. *Phys. Rev. B* **74,** 195312 (2006).
47. Lee, P. J. *et al.* Sublattice addressing and spin-dependent motion of atoms in a double-well lattice. *Phys. Rev. Lett.* **99,** 020402 (2007).
48. Zhang, S.-C. & Hu, J. A four-dimensional generalization of the quantum Hall effect. *Science* **294,** 823–828 (2001).
49. Nakajima, S. *et al.* Topological Thouless pumping of ultracold fermions. http://dx.doi.org/10.1038/nphys3622 (in the press).

Acknowledgements

We acknowledge insightful discussions with F. Grusdt and S. Kohler. This work was supported by NIM and the EU (UQUAM, SIQS). M.L. was additionally supported by ExQM and O.Z. by the Swiss National Science Foundation.

Author contributions

M.L., C.S. and M.A. performed the experiment and the data analysis. All authors contributed to the theoretical analysis and to the writing of the paper. I.B. supervised the project.

Additional information

Supplementary information is available in the online version of the paper. Reprints and permissions information is available online at www.nature.com/reprints. Correspondence and requests for materials should be addressed to M.L.

Competing financial interests

The authors declare no competing financial interests.

Methods

Initial state preparation in the first band. All sequences started by loading an $n=1$ Mott insulator of about 3,000 ^{87}Rb atoms in the lowest band of a 3D optical lattice. The lattice was created by three orthogonal standing waves with wavelengths $\lambda_l = 1{,}534$ nm for the long lattice along the x-direction and $\lambda_y = 767$ nm and $\lambda_z = 844$ nm along the y and z axes, respectively. They were ramped up in 150 ms to a depth of $V_i = 30(1)E_{r,i}, i \in \{l, y, z\}$. The superlattice potential was created by adding another lattice with $\lambda_s = \lambda_l/2$ along the x direction. To prepare the atoms in the lowest band of the superlattice, the lattice sites along the x axis were split symmetrically with $\varphi = 0.00(1)\pi$ by ramping up the short lattice to $V_s = 10.0(3)E_{r,s}$ within 10 ms while simultaneously lowering V_l to $20(1)E_{r,l}$ such that $J_1 \gg J_2$. It was verified with direct band mapping measurements that the atoms are homogeneously distributed over the entire band.

Initial state preparation in the second band. For the preparation in the second band, the splitting was instead performed at $\varphi = 0.11(1)\pi$ and V_s was ramped to $30(1)E_{r,s}$. The phase was then changed non-adiabatically to $\varphi = -0.08(1)\pi$ in 20 ms to transfer all atoms to the excited band. After that, the lattices along x were lowered to $V_s = 10.0(3)E_{r,s}$ and V_l to $20(1)E_{r,l}$, respectively, in 2 ms and the phase was moved to $\varphi = 0.00(1)\pi$ in 10 ms. This brings the atoms into the excited state of symmetric double wells with almost perfect efficiency.

Sequence for pumping. The pump cycle was implemented experimentally by slightly changing the laser frequency and thereby shifting the phase φ of the long lattice along the x direction. For this, two separate lasers were used with one laser covering the range from $-0.50(1)\pi$ to $0.62(1)\pi$ and the second laser from $0.62(1)\pi$ to $1.50(1)\pi$ (see Supplementary Information).